processes

MDPI

Article

Enhancing the Liquefied Petroleum Gas Sensing Sensitivity of Mn-Ferrite with Vanadium Doping

Omar H. Abd-Elkader [1,*], Abdullah M. Al-Enizi [2], Shoyebmohamad F. Shaikh [2], Mohd Ubaidullah [2], Mohamed O. Abdelkader [3] and Nasser Y. Mostafa [4]

[1] Department of Physics and Astronomy, College of Science, King Saud University, P.O. Box 2455, Riyadh 11451, Saudi Arabia
[2] Department of Chemistry, College of Science, King Saud University, P.O. Box 2455, Riyadh 11451, Saudi Arabia
[3] Department of Biochemistry, College of Science, King Saud University, P.O. Box 2455, Riyadh 11451, Saudi Arabia
[4] Department of Chemistry, Faculty of Science, Suez Canal University, Ismailia 41522, Egypt
* Correspondence: omabdellkader7@ksu.edu.sa

Abstract: Mn-Ferrite with a nanostructure is a highly valuable material in various technological fields, such as electronics, catalysis, and sensors. The proposed article presents the hydrothermal synthesis of Mn-ferrite doped with V (V) ions. The range of the doping level was from 0.0 to x to 0.20. The fluctuation in tetrahedral and octahedral site occupancies with Fe (III), Mn (II), and V (V) ions was coupled to the variation in unit cell dimensions, saturation magnetization, and LPG sensing sensitivity. The total magnetic moment shows a slow decrease with V-doping up to x = 0.1 (M_s = 51.034 emu/g), then sharply decreases with x = 0.2 (M_s = 34.789 emu/g). The dimension of the unit cell increases as x goes up to x = 0.1, then lowers to x = 0.2. As the level of V (V) ion substitution increases, the microstrain (ε) also begins to rise. The ε of a pure $MnFe_2O_4$ sample is 3.4 × 10^{-5}, whereas for $MnFe_{2-1.67\,x}V_xO_4$ (x = 0.2) it increases to 28.5 × 10^{-5}. The differential in ionic sizes between V (V) and Fe (III) and the generation of cation vacancies contribute to the increase in ε. The latter is created when a V (V) ion replaces 1.6 Fe (III) ions. V-doped $MnFe_2O_4$ displays improved gas-sensing ability compared to $MnFe_2O_4$ at lower operating temperature. The maximum sensing efficiency was observed for 2 wt% V-doped $MnFe_2O_4$ at a 200 °C optimum operating temperature.

Keywords: $MnFe_2O_4$; V-doping; magnetic properties; LPG sensing; magnetic properties

Citation: Abd-Elkader, O.H.; Al-Enizi, A.M.; Shaikh, S.F.; Ubaidullah, M.; Abdelkader, M.O.; Mostafa, N.Y. Enhancing the Liquefied Petroleum Gas Sensing Sensitivity of Mn-Ferrite with Vanadium Doping. *Processes* **2022**, *10*, 2012. https://doi.org/10.3390/pr10102012

Academic Editor: Fabio Carniato

Received: 31 July 2022
Accepted: 30 September 2022
Published: 5 October 2022

1. Introduction

Significant research topics focusing on safety in the environmental and industrial sectors include the establishment of gaseous and volatile liquid sensors [1]. LPG is regarded as a vital but hazardous gas in the home, especially in countries with home-gas pipeline infrastructure. Generally, flammable LPG is mainly composed of propane and butane, with few other minor hydrocarbons. LPG is used worldwide for domestic uses and as fuel for vehicles. Accidents due to odorless gas leakage are a significant problem. The number of accidents is higher in countries where liquefied petroleum gas (LPG) is supplied to homes via a pipeline network. Hence, development of a low-cost and efficient LPG sensor is important for saving homes [2].

The design of gas sensors commonly considers different sensing technologies, including chemiresistive [3], optical fiber [4], and potential sensors [5]. Metal oxide semiconductors are the essential sensing materials in sensors. Chemiresistor sensors have the advantages of simplicity and low cost. However, their major drawback is their sensitivity and selectivity. The gas-sensing mechanism involves changing material properties with the analyte concentration. This commonly occurs due to physical or chemical adsorption [6]. Nanomaterials are anticipated to perform crucial role in enhancing gas sensing, due to their

large surfaces, which enhance the adsorption phenomenon. The most vital operational parameters of gas sensors are response time, selectivity, sensitivity, and stability [7], in addition to bias voltage, operating temperature, and recovery time, which are important for long-term operation [2].

The popularity of chemiresistor sensors is due to their simplicity and low cost. The major scientific challenge for these sensors is to increase sensitivity and selectivity. Generally, there are two categories of gases: oxidizing gases and reducing gases. Moreover, there are two types of sensing materials: n-type semiconducting oxide and p-type semiconducting oxide materials [8]. Because the charge carrier in n-type materials is electrons, the conductance increases with reducing gases and decreases with oxidizing gases. The reverse occurs with p-type semiconducting sensing materials [8]. The rational selections of metal doping can be used to tune the selectivity for certain gaseous species, i.e., multi-valence ions such as Mn and Cr can be used to increase sensitivity to reduced gases.

Spinel ferrites are an enormous group of metal oxides with various technical properties, and have the composition XY_2O_4 (X = divalent metals and Y = Fe^{3+}) [9–11]. Combining various metal ions in the spinel lattice allows changes in the magnetic [12], electrical [13], and photocatalytic properties [14] of ferrites. Ferrites with nanostructure are very valuable materials in various technological fields, such as electronics, catalysis, and sensors [11,13,15–17]. Several aspects influence the performance of ferrites in different fields. These are the microstructure, stoichiometric composition, processing method, and type and extent of doping and defects. The ferrite materials exhibit a gas-sensing efficiency towards different gases [18]. The conventional ceramic method for ferrite preparation involves mixing and heating metal oxides to high temperatures for a long period [19]. However, hydrothermal synthesis involves crystallization of ferrites from alkaline solution at low temperatures < 200 °C.

In previous studies [15,17,20], we examined several metal dopants in terms of the structure, chemical properties, and technological properties of ferrites. The magnetic and photocatalytic activity under visible light of $MgFe_2O_4$ with Mo (VI) ion doping was investigated.

The results exhibited that Mo doping produced a more effective $MgFe_2O_4$ separable photocatalyst. The creation of lattice vacancies and defects, which enhance charge separation and limit charge recombination, was the primary cause of the photocatalytic enhancement [15]. Consequently, we predicted that the vacancy and defect generation in the $CoFe_2O_4$ lattice may reduce the rapid electron-hole pair recombination and improve the visible-light photocatalytic activity. The sensing sensitivity is significantly enhanced and the working temperature is lowered when La and Ce ions are doped into $MgFe_2O_4$ [21,22].

This research focuses on the use of Mn-ferrite doped with vanadium ions for sensing. In the $MnFe_2O_4$ spinel structure, vanadium ions were employed as ferric ion substitutes. Furthermore, a scientific analysis of the effects of V (V) doping on the structure and technical specifications was conducted.

2. Materials and Methods

2.1. Materials and Preparation Route

Through hydrothermally hydrolyzing co-precipitated metal hydroxides at 180 °C for 12 h, $MnFe_2O_4$ powders were synthesized. Co-precipitated metal hydroxides were prepared by dissolving 40 mmol of ferric chloride and 20 mmol of manganic chloride in 350 mL of distilled water with 1.0 M NaOH solutions. After metal hydroxide co-precipitation, NaOH solution was used to restore the pH to 12. With the addition of distilled water, the volume was increased to 380 mL before transferring to a 590 mL Teflon-lined autoclave and heated for 12 h at 180 °C. As illustrated in Figure 1, a magnetic stirrer was utilized within the Teflon-lined autoclave to optimize the homogeneity of the synthesized ferrites. V-substituted $MnFe_2O_4$ powders were prepared by replacing 1.67_x mole of Fe (III) with $_x$ mole of V (V) ions (NH_4VO_3) in order to produce powder with the following composition: $MnFe_{2-1.67x}V_xO_4$ ($0.0 \leq x \leq 0.20$).

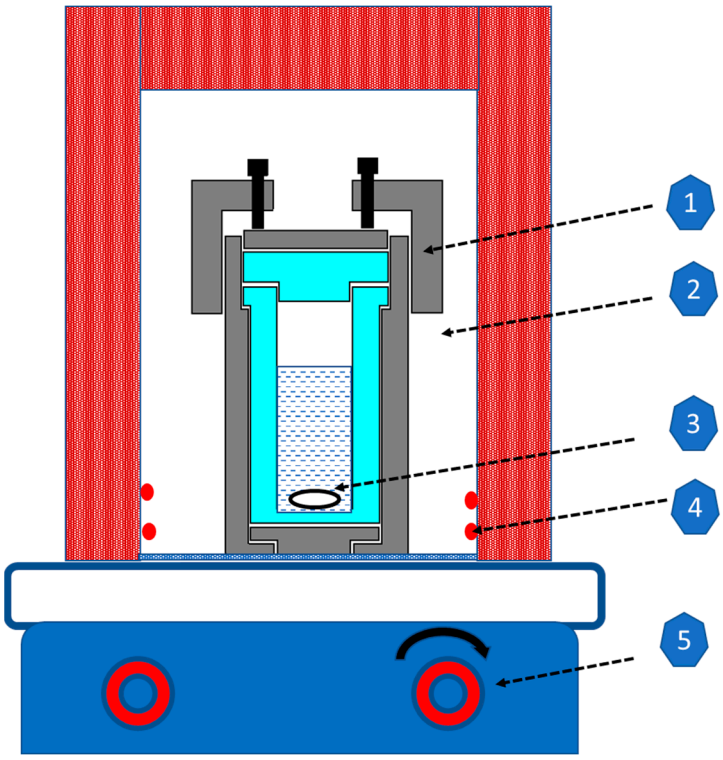

Figure 1. Hydrothermal reactor setup: (1) autoclave; (2) oven; (3) magnet; (4) heating coil; and (5) magnetic stirrer.

Centrifugation, numerous ethanol washes, and a 24 h drying period at 80 °C were all performed on the finished product.

2.2. Characterization Techniques

X-Ray diffraction (XRD) with Cu-Kα radiation were utilized in conjunction with a Brucker axis D8 diffractometer to identify crystalline phases. We used the X'Pert High Score Plus software to analyze and fit XRD patterns. The Williamson–Hall equation [6] was used to determine the ferrites crystallite sizes and microstrain (ε):

$$\beta \cos\theta = \frac{0.98\lambda}{D} + 4\varepsilon \sin\theta$$

where D is the crystallite size, β is FWHM of each peak, θ is the Bragg angle and λ is the wavelength of X-ray. Details of the W-H method were given in our recent publication [15].

The microstructure of ferrite powders was analyzed by high- resolution transmission electron microscopy (HRTEM) at a 200-kV working voltage (JTEM-2230, JEOL, Tokyo, Japan). The magnetic properties of the ferrites were investigated using a vibrating sample magnetometer (VSM) (9600-1 LDJ, Weistron Co., Ltd., West Holly-wood, CA, USA).

3. Results

3.1. XRD Analysis

XRD of Mn-ferrite incorporating different V-doping levels (x = 0.0, 0.05, 0.10, and 0.20) are shown in Figure 2. Cubic spinel ferrite phase was formed in all samples. The XRD peaks become broad with increasing amount of vanadium incorporated in ferrite (see inset of Figure 2). This broadening is due to decreasing the particle size and increasing the number of defects [15,23]. In addition, a small shift in the XRD peaks is also visible, particularly on the (311) peak highlighted in the inset of Figure 2. The unit cell dimensions of $MnFe_2O_4$ spinel with various V-doping were obtained from XRD data, as shown in Table 1. V-doping strongly affects the lattice parameter. The unit cell dimensions increase

with the increase in V-contents up to x = 0.10, then decrease with x = 0.20. These changes in unit cell dimensions result from the difference between the ionic radii of Fe (III) and that of V (V) ions in the octahedral substitution site. The ionic radii (Å) of Fe^{3+}, Mn^{2+}, and V^{5+} in both tetrahedral and octahedral sites are given in Table 2 [15]. The ionic radius of V^{5+} in octahedral sites is higher than that of Fe^{3+} in the same site. This observation indicated that V (V) substitutes the B-site. At the x = 0.2 substitution level, the most suitable explanation of the decrease in the unit cell dimensions is the redistribution of Mn (II) from the octahedral position (r = 0.83 Å) to the tetrahedral position (r = 0.66 Å). By applying the Williamson–Hall equation (W-H), the XRD data's crystallite diameters (D) and lattice strains (ε) were calculated [6]. Our most recent publications [15,24] provided a detailed explanation of the W-H technique. The determined microstrains are displayed in Table 1. The $MnFe_{2-1.67x}V_xO_4$ (x = 0.2) sample has a microstrain of 3.45 × 10^{-5} for pure $MnFe_2O_4$, which rises to 28.5 × 10^{-5}. Due to the difference in ionic volume between V^{5+} and Fe^{3+} in both octahedral and tetrahedral locations, there is a significant increase in microstrain (Table 2). Moreover, the formation of cation vacancies contributes to the increase in macrostrain. The vacancies are created to preserve the charge balance of the unit cell as one mole of V^{5+} ions replace 1.67 moles of Fe^{3+} ions, so that the produced ferrite have the general formula, $MnFe_{2-1.67x}V_xO_4$.

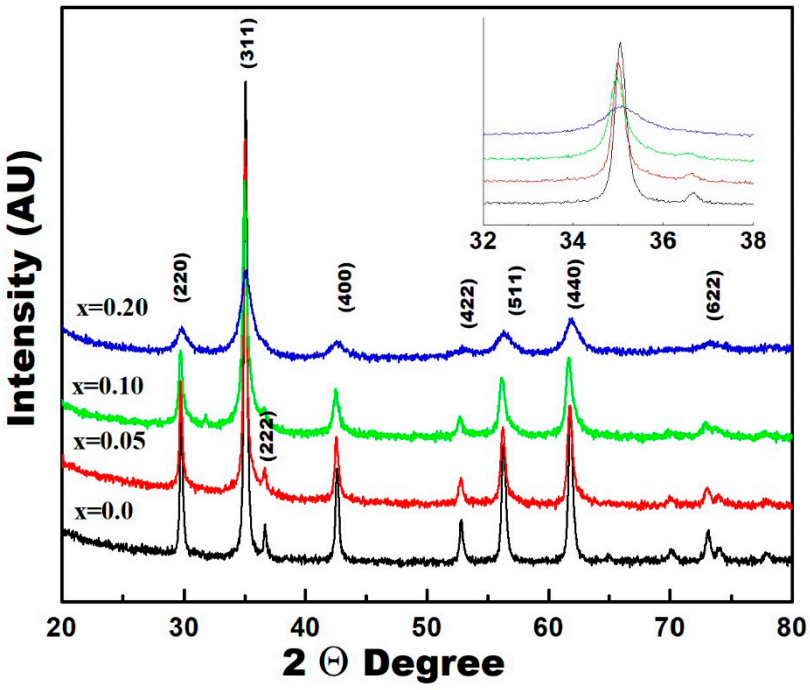

Figure 2. XRD patterns of $MnFe_{2-1.67x}V_xO_4$ spinel ferrites.

Table 1. Refined values of cell parameters *a* (Å), average crystallite size *CS* (nm) and average microstrain (με).

X Ratio	0.0	0.05	0.10	0.20
a	8.488(3)	8.490(4)	8.499(4)	8.487(6)
CS (nm)	86	25	16	6
$\varepsilon \times 10^{-5}$	3.4	9.2	19.3	28.5

Table 2. Ionic radii (Å) of metal cations in both tetrahedral and octahedral sites [15].

Metal Cation	A-Sites (Tetrahedral)	B-Sites (Octahedral)
Mn^{2+}	0.66	0.83
Fe^{3+}	0.49	0.55
V^{5+}	0.495	0.68

3.2. Microstructure Analysis

The crystallite size and shape were studied by HRTEM working at 200 Kev, as shown in Figures 3–6. The insets of the previous figures show the particle size distributions, which are in the ranges from 40 to 130 nm for all samples. The low-resolution magnifications of all samples (Figures 3–6) indicates the non-agglomerated and highly dispersed nature of all ferrite samples prepared by hydrothermal processing, which is one of the advantages of this processing route. $MnFe_2O_4$, $MnV_{0.05}Fe_{1.92}O_4$, $MnV_{0.1}Fe_{1.83}O_4$, and $MnV_{0.2}Fe_{1.67}O_4$ powders have average particle sizes of around 77, 74, 71, and 79 nm, respectively, which are in-line with those predicted by XRD analysis (Table 1). Additionally, all of the samples' high-resolution magnifications (Figures 3–6) show that they are all crystalline in form. The lattice planes in all samples are perfect and have varied spacing; for example, 0.250 nm corresponds to (311) lattice planes, whereas 0.480 nm corresponds to (111) lattice planes.

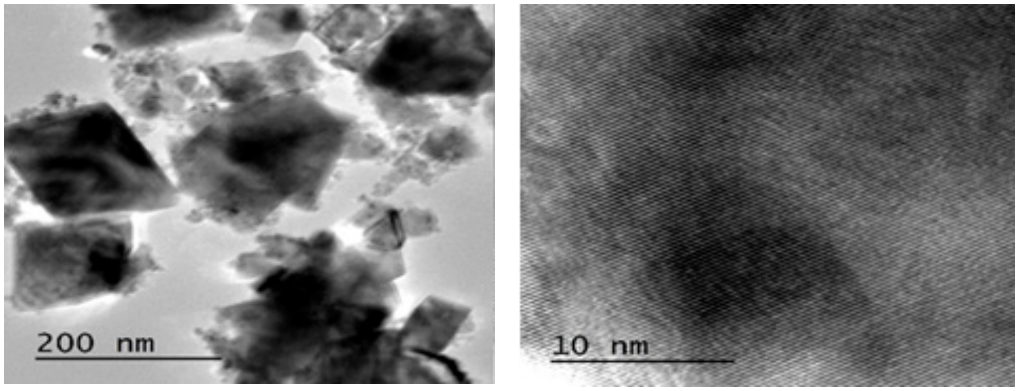

(**a**) (**b**)

Figure 3. (**a**) TEM and (**b**) HRTEM images of $MnFe_2O_4$ prepared by hydrothermal processing at 180 °C.

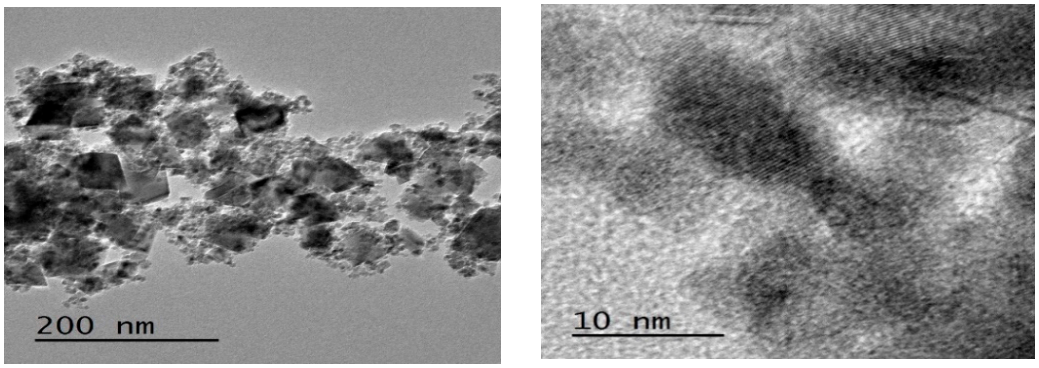

(**a**) (**b**)

Figure 4. (**a**) TEM and (**b**) HRTEM images of $MnV_{0.05}Fe_{1.92}O_4$ prepared by hydrothermal processing at 180 °C.

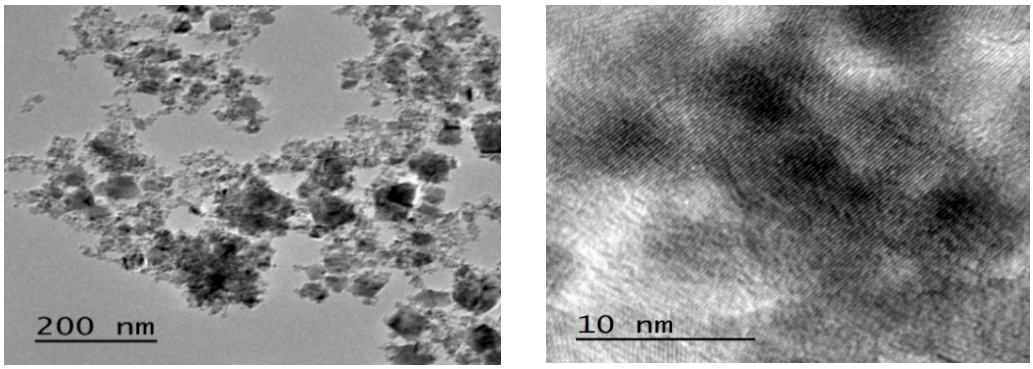

(**a**) (**b**)

Figure 5. (**a**) TEM and (**b**) HRTEM images of $MnV_{0.1}Fe_{1.83}O_4$ prepared by hydrothermal processing at 180 °C.

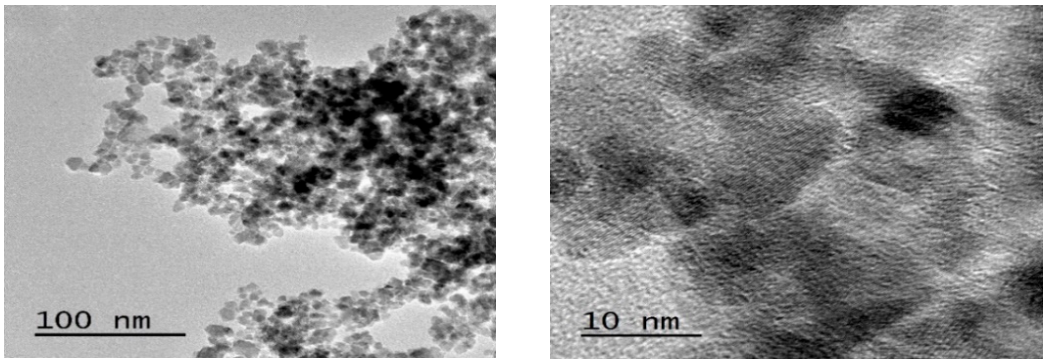

(**a**) (**b**)

Figure 6. (**a**) TEM and (**b**) HRTEM images of $MnV_{0.2}Fe_{1.67}O_4$ prepared by hydrothermal processing at 180 °C.

3.3. Magnetic Properties

By analyzing the H-M hysteresis loop at room temperature, as shown in Figure 7, the magnetic properties of vanadium-doped $MnFe_2O_4$ were investigated. The hysteresis loop of soft magnetic material is visible in all samples. The saturation magnetization of pure $MnFe_2O_4$ produced by the hydrothermal technique is 58.35 emu/g.

The variations in the H-M loops of the V-doped $MnFe_2O_4$ can be attributed to the shift in the metal ion occupancy results from V^{+5} substitution for Fe^{+3} ions in spinel lattice. Metal ions distribute in the $MnFe_2O_4$ spinel lattice, and the total magnetic moment is due to the difference in the magnetic moments of ions in octahedral positions and those in tetrahedral positions (μ = μB-site—μA-site). In pure $MnFe_2O_4$, Fe^{+3} ions are distributed partially in octahedral and tetrahedral positions. The total net magnetization results from the difference between tetrahedral (A) and octahedral (B) sublattice magnetization. Thus, the saturation magnetization (Ms) is expected to change with any change in ionic distributions between the sublattices. In the present system, XRD analysis suggested that V^{+5} ions replace Fe^{+3} in octahedral positions (B-site); thus, the total magnetic moments in B-sites decrease more than those in A-Sites, and Ms decreases. Thus, by increasing the V-doping level, Ms dramatically decreases to 34.79 emu/g at x = 0.2 (see Figure 8 and Table 3).

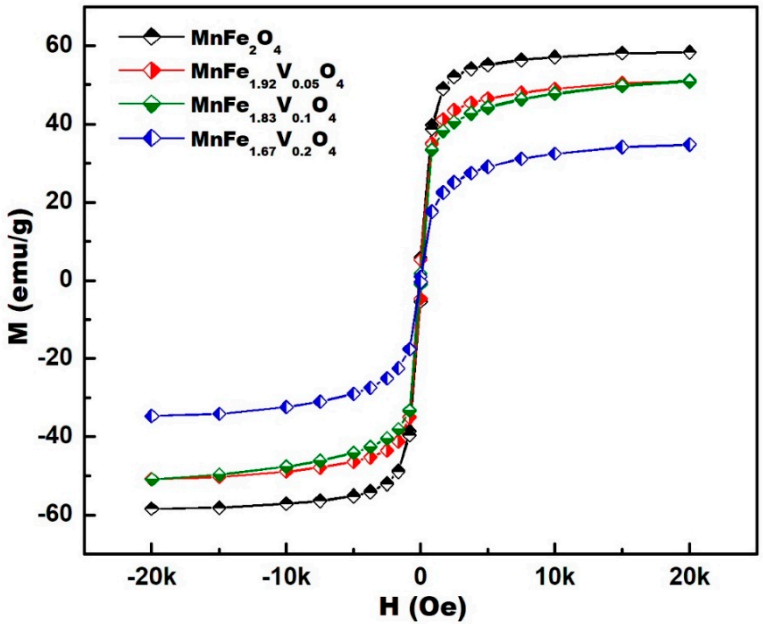

Figure 7. H-M hysteresis loops of $MnFe_{2-1.67x}V_xO_4$ spinel ferrite system hydrothermally synthesized at 180 °C.

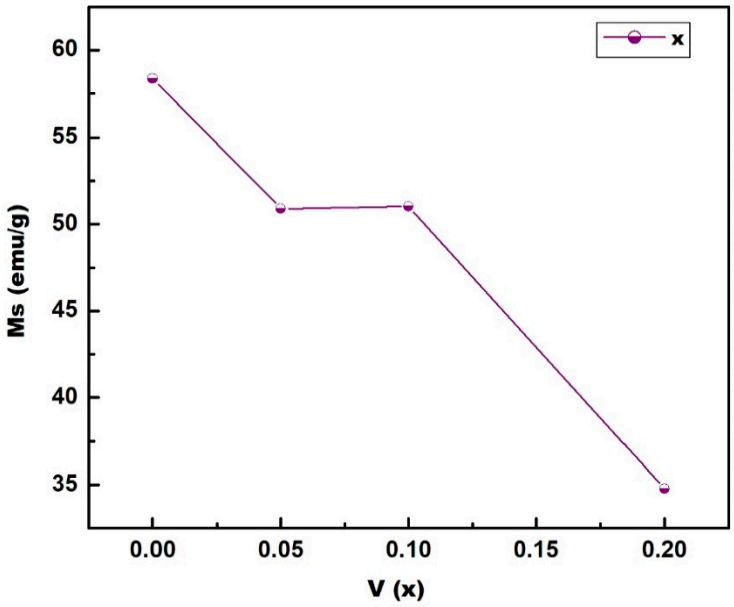

Figure 8. The change in Ms with change in V-doping level.

Table 3. Ferromagnetic parameters: saturation magnetization M_s (emu/g), Remnant magnetization M_r (emu/g), Coercivity H_c (G), and total area of hysteresis loop TA (erg/g) $\times 10^{-3}$ for $MnFe_{2-1.67x}V_xO_4$.

X ratio	0.0	0.05	0.10	0.2
H_c	106.27	104.13	32.125	31.234
M_r	5.6453	4.9897	1.3393	0.68678
M_s	58.351	50.891	51.034	34.789
TA	73.201	62.929	61.260	31.351

3.4. LPG Gas Sensing

Operating temperature (OPT) is an important factor that regulates the sensor reliability for field applications. In the current investigation, OPT was determined for each V-doped $MnFe_2O_4$ sample. The sample resistance was measured at various temperatures and fixed gas concentration of 1000 ppm.

Sensor response is expressed (%) = $(R_A - R_G) \div R_A \times 100$, where R_A is the sensor resistance in air, and R_G it's in the presence of test gas at the same temperature. The gas sensing response of several doped ferrites ($MnFe_{2-1.67\times}V_{\times}O_4$) at various operating temperatures is shown in Figure 9.

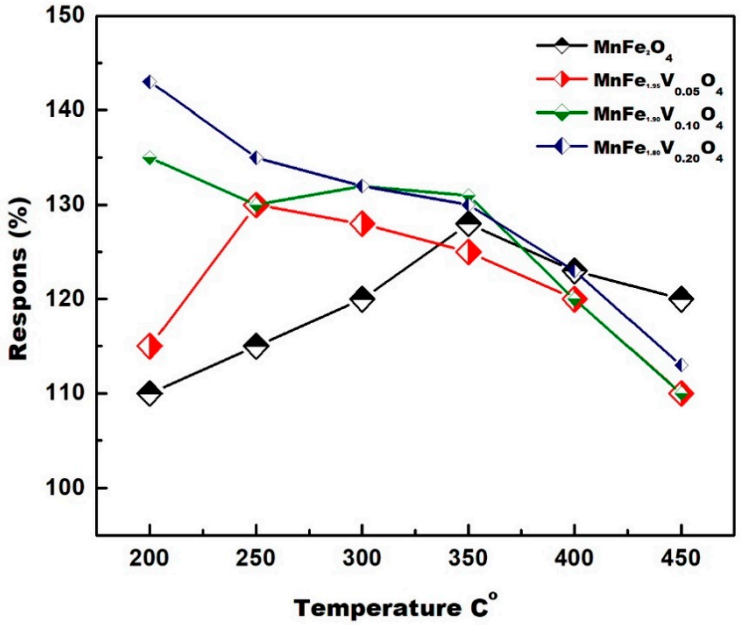

Figure 9. Variation in sensor response with operating temperature; $MnV_xFe_{1-x}O_4$ (x = 0.05, 0.1, and 0.2).

The sensing response of $MnFe_2O_4$ sensor gradually increases with the operating temperature and reaches its maximum at 350 °C. However, with further increase in temperature, the sensor response decreases. Generally, as the V-doping increased, the optimum sensing temperature shifted to a lower value. The $MnFe_{1.92}V_{0.05}O_4$ sample prepared by hydrothermal method shows its best response at 300 °C, whereas samples with high V-doping ($MnFe_{1.83}V_{0.1}O_4$ and $MnFe_{1.67}V_{0.2}O_4$ samples) show optimum temperature at 200 °C. It is obvious that increasing the amount of doping increases the sensitivity of $MnFe_2O_4$. V-doping creates vacancies and defects in $MnFe_2O_4$ lattices due to the high-charged ions; V^{+5} substitutes for 1.67 Fe/(III) ions. Thus, each V^{+5} doping produces 0.67 vacant sites in ferrite lattice. Defects and vacancies increase sensitivity due to increasing the gas adsorption ability. Abd-Elkader et al. [6] demonstrated that the response and sensitivity of $CoFe_2O_4$ for acetone, ethanol, and ammonia increases with increasing doping and defects. Moreover, Kadu et al. [25] observed that the optimum working temperature decreased with ionic substitution in a Zn ferrite system. This behavior can be explained by the reaction mechanism of hydrocarbon with surface oxygen O^{2-} ions [26].

The ferrite sensor responses at different PLG concentrations and fixed optimum temperature (200 °C) are shown in Figure 10. All ferrite samples exhibited a similar behavior of response with different LPG concentrations. The sensor responses increase by increasing the gas concentrations in a semi-linear mode. The $MnFe_{1.67}V_{0.2}O_4$ sample with the highest V-doping shows the maximum values of sensor response. The current investigation demonstrated the potential use of V-doped $MnFe_2O_4$ as a low-temperature domestic LPG gas sensor. The main component of natural gas is methane (CH_4), whereas LPG is composed

of a propane (C_3H_8) and butane (C_4H_{10}) mixture. According to Deepty et al. [26], the mechanism of ferrite sensor response to LPG analyte can represented as follows:

$$C_3H_8 + 10O^- \rightarrow 3CO_2 + 4H_2O + 10e^-$$

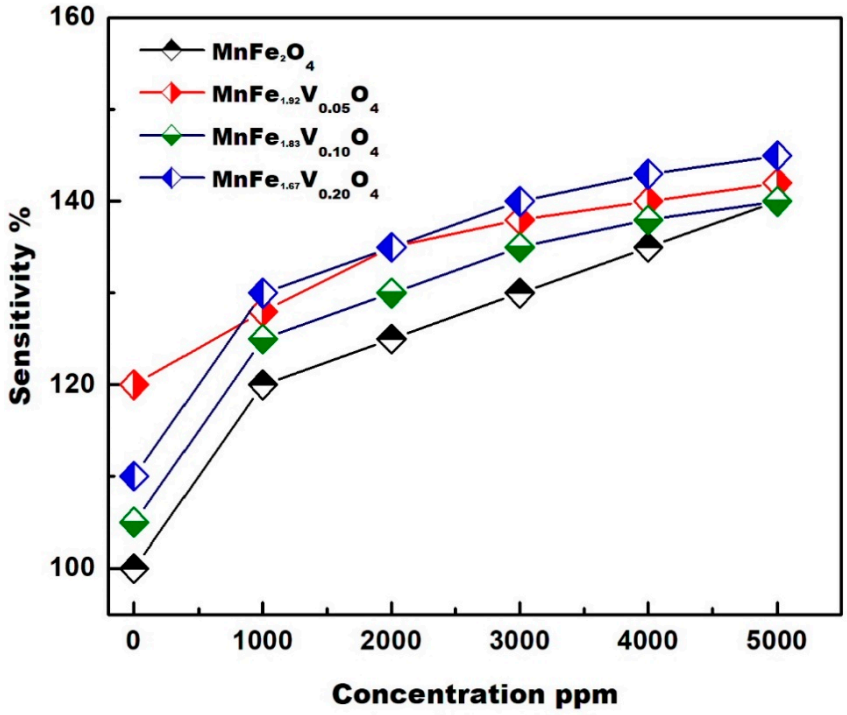

Figure 10. Variation in sensor response with different LPG concentrations at 200 °C; $MnFe_{1-1.67x}$ V_xO_4 (x = 0.05, 0.1, and 0.2).

The enhancement in sensitivity of V-doped Mn-Ferrites can be explained from the perspective of the change in the surface area and defects on the surface of ferrite with V-doping. The increase in surface area and surface defects offers more catalytic active sites for hydrocarbon oxidation reactions.

4. Conclusions

The growth in home and vehicle liquefied petroleum gas (LPG) pipeline systems has increased leakage risk, which has induced the public and scientific community to search for better leakage-detection devices [2]. Hazardous gases and different volatile liquids used in industry, and all gases leaked to the environment, need continuous monitoring. Sensors act as the first guard in the defense system against catastrophic gas leaks. In this respect, nanopolycrystalline $MnFe_2O_4$ spinel with V-doping (x = 0, 0.05, 0.1 and 0.2) was synthesized by a hydrothermal technique. The change in structure, strain, magnetic, and optical properties, and LPG gas sensing capability, were correlated with the presence of V-doping. Purity and single-phase samples were found in all examined doping ranges (0.0 × 0.2) according to XRD and HRTEM. The redistribution of Fe^{+3} ions between tetrahedral and octahedral sites caused by V^{+5} ion doping seems to cause a change in unit cell dimensions and saturation magnetization with V-doping. This is because 1.67 Fe(III) ions were replaced by 1.67 V(V) ions; however V(V), only occupied one space while leaving the other unoccupied The total saturation magnetization decreased, and the unit cell dimensions decreased, with V-substitution up to x = 0.2 (Ms = 34.8 emu/g). The pure $MnFe_2O_4$ sensor has an optimum working temperature of 350 °C. $MnFe_2O_4$ sensitivity increased and working temperature decreased to 200 °C with x = 0.1 and 0.2 doping. When compared to the parent $MnFe_2O_4$, the doping of Mn-ferrite with V greatly enhances the sensitivity of LPG detection and lowers the sensor operating temperature to 200 °C. The enhancement of V-doped

$MnFe_2O_4$ sensing for LPG can be credited to the increase in hydrocarbon chemisorption on nanostructure ferrites and the increase in the catalytic active sites.

Author Contributions: Conceptualization N.Y.M., O.H.A.-E.; methodology, S.F.S., M.U. and O.H.A.-E.; software, O.H.A.-E.; validation, N.Y.M., O.H.A.-E.; formal analysis, N.Y.M., O.H.A.-E., as well as A.M.A.-E.; investigation, N.Y.M. and O.H.A.-E.; inquiry, N.Y.M.; resources, N.Y.M., A.M.A.-E. and O.H.A.-E.; data curation, S.F.S., M.U. and M.O.A.; writing original preparation of the draft, N.Y.M. and O.H.A.-E.; writing—review and editing, N.Y.M. and O.H.A.-E.; visualization, N.Y.M. and O.H.A.-E.; supervision, N.Y.M. and O.H.A.-E.; project administration, A.M.A.-E. and O.H.A.-E.; funding acquisition, O.H.A.-E. All authors have read and agreed to the published version of the manuscript.

Funding: This Project was funded by the National Plan for Science, Technology and Innovation (MAARIFAH), King Abdulaziz City for Science and Technology, Kingdom of Saudi Arabia, Award Number (13-ADV 1478-02).

Data Availability Statement: The data presented in this study are available on request from the corresponding author.

Acknowledgments: The authors would like to extend their sincere appreciation to National Plan for Science, Technology and Innovation (MAARIFAH), King Abdulaziz City for Science and Technology, Kingdom of Saudi Arabia, Award Number (13-ADV 1478-02).

Conflicts of Interest: The authors declare no conflict of interest.

References

1. Njoroge, M.A.; Kirimi, N.M.; Kuria, K.P. Spinel ferrites gas sensors: A review of sensing parameters, mechanism and the effects of ion substitution. *Crit. Rev. Solid State Mater. Sci.* **2021**, 1–30. [CrossRef]
2. Muthuvinayagam, A.; Dhara, S. Enhanced LPG sensing property of sol–gel synthesized ZnO nanoparticles-based gas sensors. *Bull. Mater. Sci.* **2021**, *44*, 159. [CrossRef]
3. Madake, S.B.; Hattali, M.R.; Thorat, J.B.; Pedanekar, R.S.; Rajpure, K.Y. Chemiresistive Gas Sensing Properties of Copper Substituted Zinc Ferrite Thin Films Deposited by Spray Pyrolysis. *J. Electron. Mater.* **2021**, *50*, 2460–2465. [CrossRef]
4. Hernández, P.T.; Kuznetsov, M.V.; Morozov, Y.G. High-Temperature Synthesis of Nickel-Based Nanoparticles for Use as Materials in Sensors of Potentially Hazardous Gases. *Int. J. Self Propagating High Temp. Synth.* **2019**, *28*, 159–172. [CrossRef]
5. Matatagui, D.; Bahos, F.A.; Gràcia, I.; Horrillo, M.C. Portable low-cost electronic nose based on surface acoustic wave sensors for the detection of BTX vapors in air. *Sensors* **2019**, *19*, 5406. [CrossRef]
6. Abd-Elkader, O.H.; Al-enizi, A.M.; Shaikh, S.F.; Ubaidullah, M.; Abdelkader, M.O.; Mostafa, N.Y. The Structure, Magnetic, and Gas Sensing Characteristics of W-Substituted Co-Ferrite Nanoparticles. *Crystals* **2022**, *12*, 393. [CrossRef]
7. Sankaran, K.J.; Suman, S.; Sahaw, A.; Balaji, U.; Sakthivel, R. Improved LPG sensing properties of nickel doped cobalt ferrites derived from metallurgical wastes. *J. Magn. Magn. Mater.* **2021**, *537*, 168231. [CrossRef]
8. Shozi, N.N.; Kortidis, I.; Mkwae, P.S.; Chonco, N.P.; Leshabane, N.; Jozela, M.; Kroon, R.E.; Swart, H.C.; Nkosi, S.S. Extremely sensitive and selective flammable liquefied hydrocarbon gas sensing and inter-dependence of fluctuating operating temperature and resistance: Perspective of rare-earth doped cobalt nanoferrites. *J. Alloy. Compd.* **2021**, *859*, 157846. [CrossRef]
9. El-Shobaky, G.A.; Turky, A.M.; Mostafa, N.Y.; Mohamed, S.K. Effect of preparation conditions on physicochemical, surface and catalytic properties of cobalt ferrite prepared by coprecipitation. *J. Alloy. Compd.* **2010**, *493*, 415–422. [CrossRef]
10. Aljuraide, N.I.; Mousa, M.A.A.; Mostafa, N.Y.; El-Shobaky, G.A.; Hamdeh, H.H. Microstructure analysis of zinc ferrite nanoparticles by means of X-ray powder diffraction and Mössbauer spectroscopy. *Int. J. Nanoparticles* **2012**, *5*, 56–63. [CrossRef]
11. Mostafa, N.Y.; Hessien, M.M.; Shaltout, A.A. Hydrothermal synthesis and characterizations of Ti substituted Mn-ferrites. *J. Alloy. Compd.* **2012**, *529*, 29–33. [CrossRef]
12. Hemeda, O.M.; Mostafa, N.Y.; Abd Elkader, O.H.; Ahmed, M.A. Solubility limits in Mn–Mg ferrites system under hydrothermal conditions. *J. Magn. Magn. Mater.* **2014**, *364*, 39–46. [CrossRef]
13. Hemeda, O.M.; Mostafa, N.Y.; Abd Elkader, O.H.; Hemeda, A.; Tawfik, A. Electrical and morphological properties of magnetocaloric nano ZnNi ferrite. *J. Magn. Magn. Mater.* **2015**, *394*, 96–104. [CrossRef]
14. Mezni, M.; Ibrahim, M.M.; El-Kemary, M.; Shaltout, A.A.; Mostafa, N.Y.; Ryl, J.; Kumeria, T.; Altalhi, T.; Amin, M.A. Cathodically activated Au/TiO_2 nanocomposite synthesized by a new facile solvothermal method: An efficient electrocatalyst with Pt-like activity for hydrogen generation. *Electrochim. Acta* **2018**, *290*, 404–418. [CrossRef]
15. Ahmed, S.I.; Heiba, Z.K.; Mostafa, N.Y.; Shaltout, A.A.; Aljoudy, H.S. The role of high-valent (Mo and V) cations in defect spinel iron oxide nanomaterials: Toward improving Li-ion storage. *Ceram. Int.* **2018**, *44*, 20692–20699. [CrossRef]
16. Heiba, Z.K.; Mostafa, N.Y.; Abd-Elkader, O.H. Structural and magnetic properties correlated with cation distribution of Mo-substituted cobalt ferrite nanoparticles. *J. Magn. Magn. Mater.* **2014**, *368*, 246–251. [CrossRef]
17. Mostafa, N.Y.; Mahmoud, M.H.; Heiba, Z.K. Hydrolysis of $TiOCl_2$ leached and purified from low-grade ilmenite mineral. *Hydrometallurgy* **2013**, *139*, 88–94. [CrossRef]

18. Srinivasamurthy, K.M.; Manjunatha, K.; El-Denglawey, A.; Rajaramakrishna, R.; Kubrin, S.P.; Pasha, A.V.; Angadi, V.J. Evaluation of structural, dielectric and LPG gas sensing behavior of porous Ce^{3+}-Sm^{3+} doped Cobalt nickel ferrite. *Mater. Chem. Phys.* **2022**, *275*, 125222. [CrossRef]
19. Mosstafa, K.; Massoud, G.; Ali, M. Cobalt ferrite nanoparticles ($CoFe_2O_4$ MNPs) as catalyst and support: Magnetically recoverable nanocatalysts in organic synthesis. *Nanotechnol. Rev.* **2018**, *7*, 43–68.
20. Heiba, Z.K.; Mohamed, M.B.; Mostafa, N.Y.; El-Naggar, A.M. Structural and Optical Properties of $Cd_{1-x}Mn_xFe_2O_4$/PMMA Nanocomposites. *J. Inorg. Organomet. Polym. Mater.* **2020**, *30*, 1898–1906. [CrossRef]
21. Patil, J.Y.; Nadargi, D.Y.; Mulla, I.S.; Suryavanshi, S.S. Cerium doped $MgFe_2O_4$ nanocomposites: Highly sensitive and fast response-recoverable acetone gas sensor. *Heliyon* **2019**, *5*, e01489. [CrossRef] [PubMed]
22. Yadav, A.K.; Singh, R.K.; Singh, P. Fabrication of lanthanum ferrite based liquefied petroleum gas sensor. *Sens. Actuators B Chem.* **2016**, *229*, 25–30. [CrossRef]
23. Mezni, A.; Ben Saber, N.; Ibrahim, M.M.; Shaltout, A.A.; Mersal, G.A.; Mostafa, N.Y.; Alharthi, S.; Boukherroub, R.; Altalhi, T. Pt–ZnO/M (M=Fe, Co, Ni or Cu): A New Promising Hybrid-Doped Noble Metal/Semiconductor Photocatalysts. *J. Inorg. Organomet. Polym. Mater.* **2020**, *30*, 4627–4636. [CrossRef]
24. Zaki, Z.I.; Alotaibi, S.H.; Alhajji, B.A.; Mostafa, N.Y.; Amin, M.A.; Mohsen, Q. ZrN/$ZrSi_2$/Co Cermet by Combustion Synthesis under Pressure: Influence of Co Addition. *Int. J. Self Propagating High Temp. Synth.* **2020**, *29*, 225–232. [CrossRef]
25. Kadu, A.V.; Jagtap, S.V.; Chaudhari, G.N. Studies on the preparation and ethanol gas sensing properties of spinel $Zn_{0.6}Mn_{0.4}Fe_2O_4$ nanomaterials. *Curr. Appl. Phys.* **2009**, *9*, 1246–1251. [CrossRef]
26. Deepty, M.; Srinivas, C.; Ranjith Kumar, E.; Ramesh, P.N.; Mohan, N.K.; Sher Singh, M.; Prajapat, C.L.; Verma, A.; Sastry, D. Evaluation of structural and dielectric properties of Mn^{2+}-substituted Zn-spinel ferrite nanoparticles for gas sensor applications. *Sens. Actuators B Chem.* **2020**, *316*, 128127.